



# 1 **Subsurface manifestation of Marine Heatwaves in the South West** 2 **Indian Ocean**

3 Clea B. Welch<sup>1,2</sup>, Neil Malan<sup>3</sup>, Daneeja Mawren<sup>1,2</sup>, Tamaryn Morris<sup>2</sup>, Janet Sprintall<sup>4</sup>, Juliet C. Hermes<sup>1,2</sup>

4 <sup>1</sup>Ocean and Atmosphere Science, University of Cape Town, Cape Town, 7700, South Africa

5 <sup>2</sup>South African Environmental Observation Network Egagasini node, Cape Town, South Africa

6 <sup>3</sup>Climate Change Research Centre and Centre of Marine Science and Innovation, University of New South Wales, Sydney,  
7 New South Wales, Australia

8 <sup>4</sup>Scripps Institution of Oceanography, University of California, San Diego, La Jolla, CA, United States

9 *Correspondence to:* Clea B. Welch (wlccl001@myuct.ac.za)

10 **Abstract.** Marine heatwaves (MHW) are extreme events of prolonged, anomalously warm ocean temperatures. Globally,  
11 marine heatwaves are increasing in frequency and intensity and are responsible for long-term impacts on marine ecosystems,  
12 which have devastating socio-economic consequences. A key gap in our understanding of MHWs is how they manifest in the  
13 subsurface. This paper uses satellite sea surface temperature (SST) data and *in situ* subsurface temperature observations from  
14 Expendable Bathythermographs (XBTs) to investigate the anomalous water temperature characteristics associated with surface  
15 identified MHWs in the South West Indian Ocean (SWIO) and how they progress through the water column. We find that the  
16 SWIO, which is dominated by the presence of mostly warm anticyclonic eddies, is characterised by moderate MHWs, and that  
17 the frequency, duration and intensity of these events are largely associated with mesoscale activity. Surface-detected MHW  
18 case studies demonstrated a strong subsurface temperature anomaly signal, with maximum intensity below the mixed layer  
19 depth. The spatial distribution of anticyclonic, warm-core eddies closely matched the distribution of the MHWs. This provides  
20 a possible mechanism for the deep extent of these surface MHWs. Improving our understanding of the interaction between  
21 mesoscale features and subsurface MHW characteristics will benefit prediction of MHWs and management of the regions'  
22 biodiversity.

## 23 **1 Introduction**

24 Marine heatwaves (MHWs) are extreme, anomalously warm ocean events that are known to have devastating impacts on  
25 marine species, ecosystems, and ultimately coastal countries' socioeconomics that depend on a blue economy (Mills et al.,  
26 2013; Hobday and Pecl, 2014; Hermes et al., 2019). The thermal stress during MHWs has initiated coral bleaching events,  
27 destroyed marine foundation species, caused mass mortality events, species redistributions and resulted in irreversible  
28 physiological damage to marine life (Mills et al., 2013; Frölicher et al., 2018; Oliver et al., 2021; Perez et al., 2021; Garrabou  
29 et al., 2022; Mawren, et al., 2022 b). The adverse effects of MHWs are especially concerning as, under scenarios of continued



30 global ocean warming, MHWs are projected to increase globally, with events lasting longer and intensifying. If this trend  
31 continues many parts of the ocean are predicted to reach a near-permanent MHW state by the late 21st century (Hobday et al.,  
32 2016; Frölicher et al., 2018; Oliver et al., 2018; Holbrook et al., 2020). This highlights the need for rapid improvement in our  
33 understanding of MHWs and how to manage or adapt to their impacts (Elzahaby and Schaeffer, 2019).

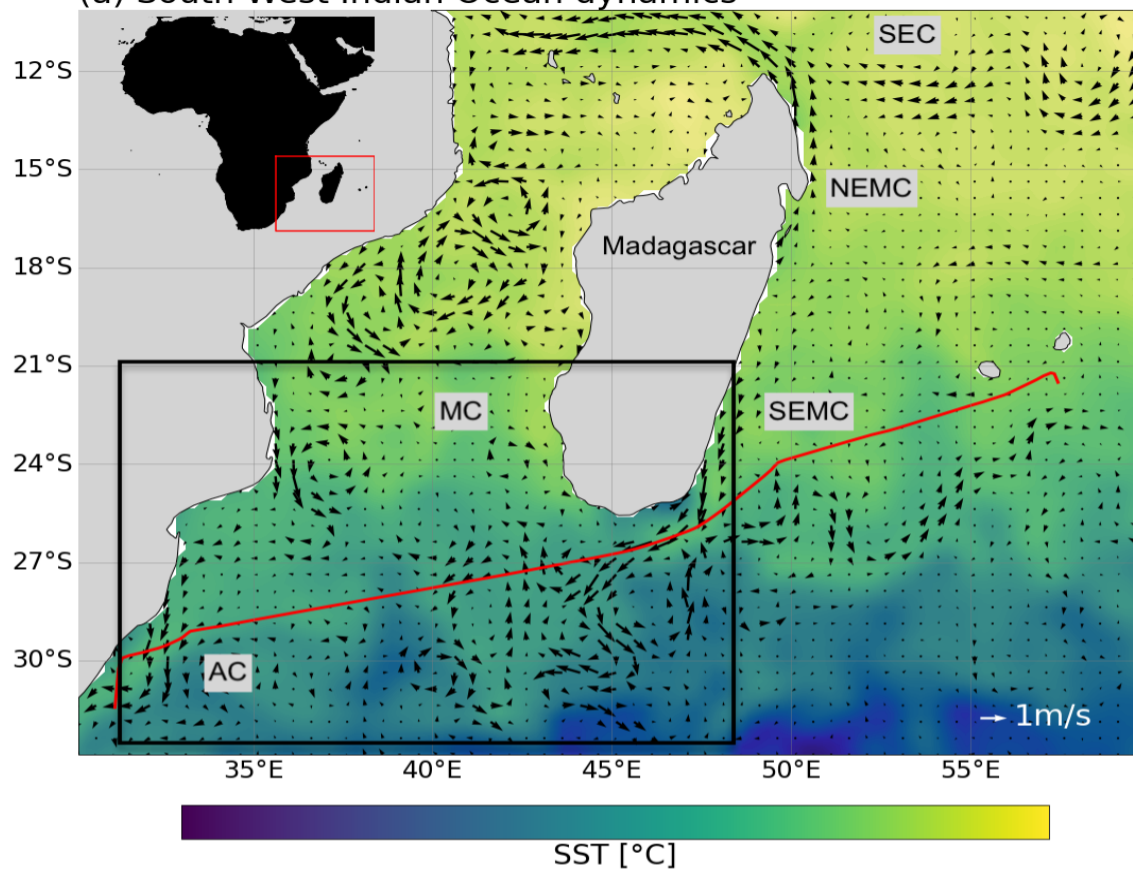
34 A key gap in our understanding of MHW events is how they manifest in the subsurface (Oliver et al., 2018). MHW detection  
35 and characterization is largely limited to the surface due to the lack of continuous, long-term, and high-resolution subsurface  
36 temperature records (Elzahaby et al., 2021). However, MHWs themselves are not surface trapped, as they can penetrate to  
37 considerable depths, or even exist at depth with no surface signal (Elzahaby and Schaeffer, 2019; Holbrook et al., 2020;  
38 Scannell et al., 2020; Elzahaby et al., 2021; Schaeffer, Sen Gupta and Roughan, 2023; Zhang et al., 2023). The lack of  
39 subsurface MHW characterisation limits our understanding of the true impacts these events have, as it is the vertical extent of  
40 MHWs that directly impact marine ecosystems (Elzahaby and Schaeffer, 2019; Holbrook et al., 2020; Scannell et al., 2020).  
41 The subsurface extent of MHWs is often associated with different spatial MHW patterns and drivers compared to the surface  
42 (Elzahaby and Schaeffer, 2019; Scannell et al., 2020; Perez et al., 2021; Fragkopoulou et al., 2023; Zhang et al., 2023).  
43 Different ocean dynamical processes, such as large-scale circulation, oceanic planetary waves, boundary currents, eddies, local  
44 downwelling, seasonal stratification and mixing influences the vertical structure of MHWs (Schaeffer, Sen Gupta and  
45 Roughan, 2023; Zhang et al., 2023). Upper ocean MHWs (0-150 m) have been shown to mostly originate from anomalous air-  
46 sea fluxes, but even in cases where air-sea heat fluxes are the predominant driver of MHWs, ocean dynamical processes can  
47 extend the warm MHW signature into the subsurface (Schaeffer, Sen Gupta and Roughan, 2023; Zhang et al., 2023). Deeper  
48 MHWs (that extend below 150m) are shown to be mostly driven by deep warm-core, anticyclonic mesoscale eddies (Schaeffer  
49 and Roughan, 2017; Elzahaby and Schaeffer, 2019; Perez et al., 2021; Fragkopoulou et al., 2023), boundary current shifts  
50 (Großelindemann et al., 2022) and Ekman pumping (Hu et al., 2021). In particular, eddies in subtropical western boundary  
51 currents (WBCs) are known to drive deeper and longer-lasting MHWs (Schaeffer and Roughan, 2017; Elzahaby and Schaeffer,  
52 2019; Benthuyzen et al., 2020; Elzahaby et al., 2021; Zhang et al., 2023).

53 Here, focus is on the South West Indian Ocean (SWIO), which is part of the greater western Indian Ocean global warming  
54 hotspot (Roxy et al., 2014), and is host to a highly unique, complex and variable WBC current system. To date, the  
55 characterisation of MHWs in this region is sparse and limited to the surface (Mawren et al., 2022 a). A key feature in the SWIO  
56 is the Greater Agulhas Current System which consists of the eddying flow through the Mozambique Channel (MC) and two  
57 dynamic WBCs, the South East Madagascar Current (SEMC) and the Agulhas Current (AC), the largest and strongest Southern  
58 Hemisphere WBC, which plays a vital role in global thermohaline circulation (Fig. 1; Beal et al., 2020). Flow through the MC  
59 is characterised by large, deep-reaching, mostly anticyclonic and anomalously warm southward propagating mesoscale eddies,  
60 which are formed from baroclinic instability in the South Equatorial Current (SEC), around the Comoros Islands (Collins,  
61 Reason and Hermes, 2012; Halo et al., 2014; Voldsund et al., 2017). South of Madagascar, the SEMC retroflects and sheds  
62 pairs of counter-rotating mesoscale eddies which converge with eddies from the MC (Voldsund et al., 2017). The persistence  
63 of eddies from the MC and SEMC creates a state of instability, which is the main source of variability and SST anomalies in

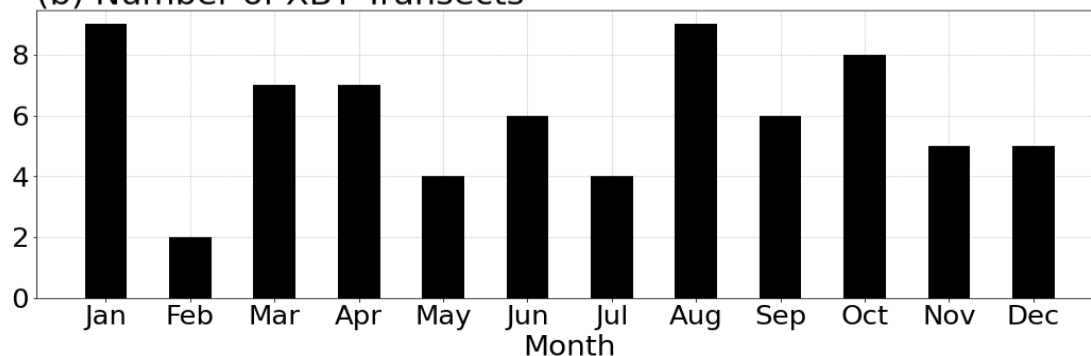


64 the region, making this region especially susceptible to the occurrence of MHWs (DiMarco, Chapman and Nowlin, 2000;  
 65 Halo et al., 2014; Phillips et al., 2021; Mawren et al., 2022 a).

(a) South West Indian Ocean dynamics



(b) Number of XBT Transects



66

67 **Figure 1:** (a) A snapshot of sea surface temperature conditions on 13/04/2021 (OISST V2) of the South West Indian Ocean, with geostrophic  
 68 current velocities overlaid (satellite AVISO altimeter). Key ocean circulation features are highlighted - SEMC South-East Madagascar  
 69 Current, NEMC North-East Madagascar Current, SEC South Equatorial Current, Mozambique Channel and Agulhas Current. The black box  
 70 22° S - 32° S and 31° E - 48° E indicates the study area. The red line represents the IX21 HR-XBT transect from Durban, South Africa to  
 71 Port Louis, Mauritius. (b) The number of XBT transects available for each month from the IX21 transect for the period from 1994 – 2022.



72 Where the MC and SEMC converge, eddy activity is highest, and surface-identified MHWs are increasing in frequency,  
73 intensity and duration more rapidly than anywhere else in the MC (Mawren et al., 2022 a). Intensification of mesoscale eddies,  
74 has subsequently increased ocean warming trends and SST anomalies, which may largely explain these observed MHW trends  
75 (Wu et al., 2012; Schaeffer and Roughan, 2017; Benthuyssen et al., 2020; Mawren et al., 2022 a). The most intense and longest-  
76 lasting MHW in the MC occurred in February 2017 (Mawren et al., 2022 a). It was found to be modulated by horizontal  
77 advection and the presence of mesoscale eddies, with maximum temperature anomalies peaking when the core of an  
78 anticyclonic eddy passed through (Mawren, Hermes and Reason, 2022 a). This suggests that, as seen in other WBC regions  
79 (Bian et al., 2023), mesoscale eddies significantly influence the occurrence and intensity of MHWs in the SWIO (Mawren et  
80 al., 2022 a). Yet, the exact role mesoscale eddies play in driving surface MHW characteristics and their subsurface extent,  
81 remains unclear. This is of particular concern as the SWIO supports a variety of temperature-sensitive, pristine ecosystems  
82 with high biological diversity, high endemism and endangered species. The disruption to the ecosystem can have significant  
83 socioeconomic impacts, as neighbouring east African countries rely heavily on these ecosystems for fish stocks and marine  
84 ecotourism (Obura, 2012; Pereira et al., 2014).

85 This study aims to build on the limited work that has previously explored MHW events and trends in the SWIO with a focus  
86 on their subsurface characteristics. In Section 2, data sets and methodology are described. Section 3 investigates surface MHW  
87 characteristics, then, using temperature profiles from in situ Expendable Bathythermographs (XBTs) observations, the  
88 subsurface extent of surface-identified MHWs are explored. This provides the first description of subsurface characteristics of  
89 MHWs in the SWIO. Particular focus is also placed on understanding the role mesoscale eddies play on both the surface and  
90 subsurface extent of MHWs. For this reason, the study area is confined to 22° S - 32° S and 31° E - 48° E, which encompasses  
91 the region of greatest ocean variability and mesoscale eddy activity south and southwest of Madagascar (Fig. 1). A Discussion  
92 follows in Section 4 with Conclusions in Section 5.

## 93 **2 Methods**

### 94 **2.1 Sea surface temperature and surface marine heatwave identification**

95 High resolution gridded (0.25°) NOAA optimally interpolated sea surface temperature (OI SST) V2 data was used to explore  
96 SST conditions and identify surface MHWs in the SWIO region from 1993 – 2022. OISST data has been widely used to  
97 identify and characterise global and regional MHW events and trends globally (Reynolds et al., 2007; Banzon et al., 2016;  
98 Frölicher et al., 2018; Sen Gupta et al., 2020; Guo et al., 2022; Saranya et al., 2022) and in the SWIO (Mawren et al., 2022 a;  
99 Mawren et al., 2022 b).

100 MHWs were identified and quantified in the SWIO using the Hobday et al., (2016) definition, which defines a MHW as a  
101 discrete, anomalously warm water event, with temperatures that exceed the 90th percentile (the threshold) of the 30-year  
102 historical baseline period and have a duration of at least five consecutive days. A fixed climatological baseline and a 31 day  
103 smoothing window was used to identify surface MHWs. The properties of MHWs over the region were described by set



104 metrics: mean duration (the time, in days, between the start and end of a MHW), mean frequency (the number of events that  
105 occurred during a year or season), mean intensity (the average temperature anomaly over the duration of the event) and the  
106 cumulative intensity (integrated temperature anomaly for the duration of the event).

## 107 **2.2 Subsurface temperature measurements from *in situ* data**

108 The subsurface expression of surface MHWs (detected from OISST data) was investigated using XBT data from the near-  
109 repeat IX21 HR-XBT transect. XBTs provide temperature profiles from 0 to 850 m depth. IX21 is nominally from Durban,  
110 South Africa (29.9° S, 31.0° E) to Port Louis, Mauritius (20.2° S, 57.5° E) (Chandler, Zilberman and Sprintall, 2022), but for  
111 this study, the portion of the IX21 transect from Durban to south of Madagascar was used.

112 The IX21 HR-XBT transect is nominally occupied 4 times a year and has a horizontal resolution of 6 – 10 km between XBT  
113 profiles within the boundary current and 20-30 km offshore (Goni et al., 2019; Chandler, Zilberman and Sprintall, 2022). The  
114 transect takes three days to complete and so is considered synoptic. Each transect is assigned the date of the first temperature  
115 profile acquired for the cruise. Temperature was objectively mapped to 10m depth intervals from 0m to 800 m and 0.1°  
116 intervals in longitude (Chandler, Zilberman and Sprintall, 2022). Data was available from 8 September 1994 to 6 September  
117 2022.

118 Since XBT data from the IX21 transect is collected nominally 4 times a year, there is not enough data to produce a high-  
119 resolution climatological baseline period, which is required to identify MHWs using the Hobday et al., (2016) definition.  
120 Instead, subsurface temperature anomalies calculated relative to the seasonal climatological means, calculated using the XBT  
121 data (Fig. 1b), from 1994 – 2022 were used as the measure of the subsurface extent of surface MHWs, an approach commonly  
122 used when studying subsurface MHW signals using *in situ* data (Schaeffer and Roughan, 2017; Elzahaby and Schaeffer, 2019;  
123 Elzahaby et al., 2021; Perez et al., 2021). Each seasonal mean consisted of ~15-20 XBT transects (Fig. 1b). To calculate  
124 temperature anomalies, the seasonal climatological means were subtracted from the daily temperature profiles for each data  
125 available day.

## 126 **2.3 Sea level anomaly data**

127 To investigate the influence of mesoscale eddies on the properties of surface-identified MHWs, high resolution (0.25°),  
128 optimally integrated, gridded daily sea level anomalies (SLA) and geostrophic currents, over a twenty-year period (1993 -  
129 2012), were extracted from altimeter satellite data distributed by AVISO (Archiving, Validation, and Interpretation of Satellite  
130 Oceanographic data). This data has previously been used to track eddies during MHWs in the SWIO by Mawren et al. (2022a).  
131 In the SWIO, where *in situ* observations are sparse, satellite altimetry provides useful information about mesoscale ocean  
132 variability and is the best way to identify the presence of mesoscale eddies (Halo et al., 2014). Positive (negative) SLA  
133 associated with anticyclonic (cyclonic) geostrophic currents indicate the presence of warm-core (cold-core) eddies (Halo et  
134 al., 2014).



135 Mean eddy kinetic energy (EKE) for the entire time period was calculated using SLA and geostrophic velocity and used as a  
136 measure of eddy activity across the region. Mean EKE was calculated as:

$$137 \text{ EKE} = \frac{1}{2}(\overline{u'^2} + \overline{v'^2}), \quad (1)$$

138 where  $u'^2$  represents the mean squared anomaly of the horizontal velocity component  $u$  from its spatial mean and  $v'^2$  represents  
139 the mean squared anomaly of the vertical velocity component  $v$  from its spatial mean (Bai et al., 2024).

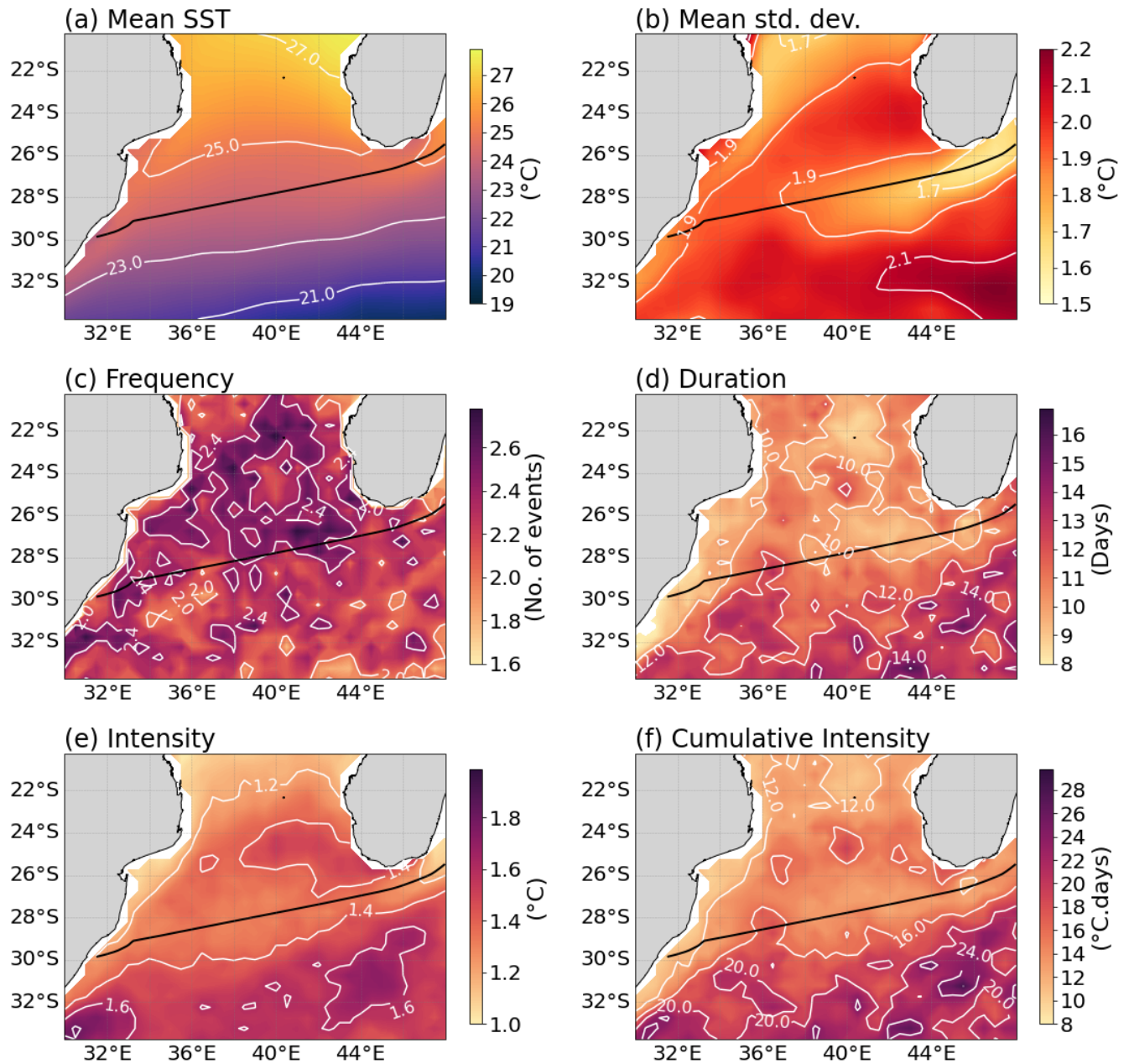
### 140 **3 Results**

#### 141 **3.1 Surface MHW variability**

142 The SWIO is defined by distinct spatial patterns of mean annual surface MHW characteristics that are underpinned by pre-  
143 existing mean SST conditions and variability (Fig. 2). On the other hand, despite distinct seasonality in mean SST and  
144 variability, MHWs do not exhibit strong seasonality, as the spatial pattern of MHW cumulative intensity remains similar during  
145 each season (Not shown). Due to the lack of observed MHW seasonality, the mean MHW trends and their relationship with  
146 SST variability and mesoscale eddies are further investigated.

147 The SWIO experiences warm mean ocean temperatures, up to 28 °C , in the Mozambique Channel (21° S) that  
148 decrease southward, reaching a minimum of 19 °C at 33° S (Fig. 2a). The SST standard deviation shows that, on average, the  
149 majority of the region experiences SSTs that exceed the mean by between 1.5 - 2.2 °C (Fig. 2b). On average, surface MHWs  
150 occur 1 to 3 times per year, last 8 – 18 days and reach intensities of 1.0 – 2.0 °C, but have varying spatial characteristics (Fig.  
151 2b – f). These observed mean values of MHW frequency, duration, intensity and cumulative intensity, are consistent with  
152 previous findings by Mawren et al. (2021) in the SWIO, and global WBC studies by Oliver et al. (2018) and Holbrook et al.  
153 (2019). Within the southern MC, MHWs occur most frequently (between 2 - 3 times on average per year), but are shorter-  
154 lived (8 -12 days) and less intense (1.2 – 1.5 °C), whereas, in the southeast open ocean region, MHWs occur less frequently  
155 (between 1 – 2 times on average per year), but are longer-lasting (12 – 18 days) and more intense (1.4 – 2.2 °C) (Fig. 2c,d).  
156 Similarly, since cumulative intensity is the integration of duration and intensity, MHWs are the most severe (16 – 19 °Cdays)  
157 in the southeast open ocean, and least severe in the southern MC (8 - 16 °Cdays) (Fig. 2f).





158

159 **Figure 2:** Climatological mean (a) SST (°C) and (b) SST standard deviation (°C). Surface mean annual MHW (c) frequency, (d) duration  
160 (days), (e) intensity (°C) and (f) cumulative intensity (°Cdays) calculated from NOAA optimally interpolated sea surface temperature (OISST  
161 V2) high resolution (0.25°) gridded SST data for the climatological period from 1993–2023. The black solid line in all the figures denotes  
162 the IX21 XBT transect.

163 The mean spatial distribution of MHW characteristics are largely related to the underlying patterns of SST variability (Fig. 2).  
164 As is seen in the mean spatial distribution of MHW intensity, SST variance is highest off the west coast of Madagascar (1.5  
165 °C) and in the southern-most open ocean (1.9 – 2.2 °C) but is weakest along the west coast of Africa and at the region of SEMC

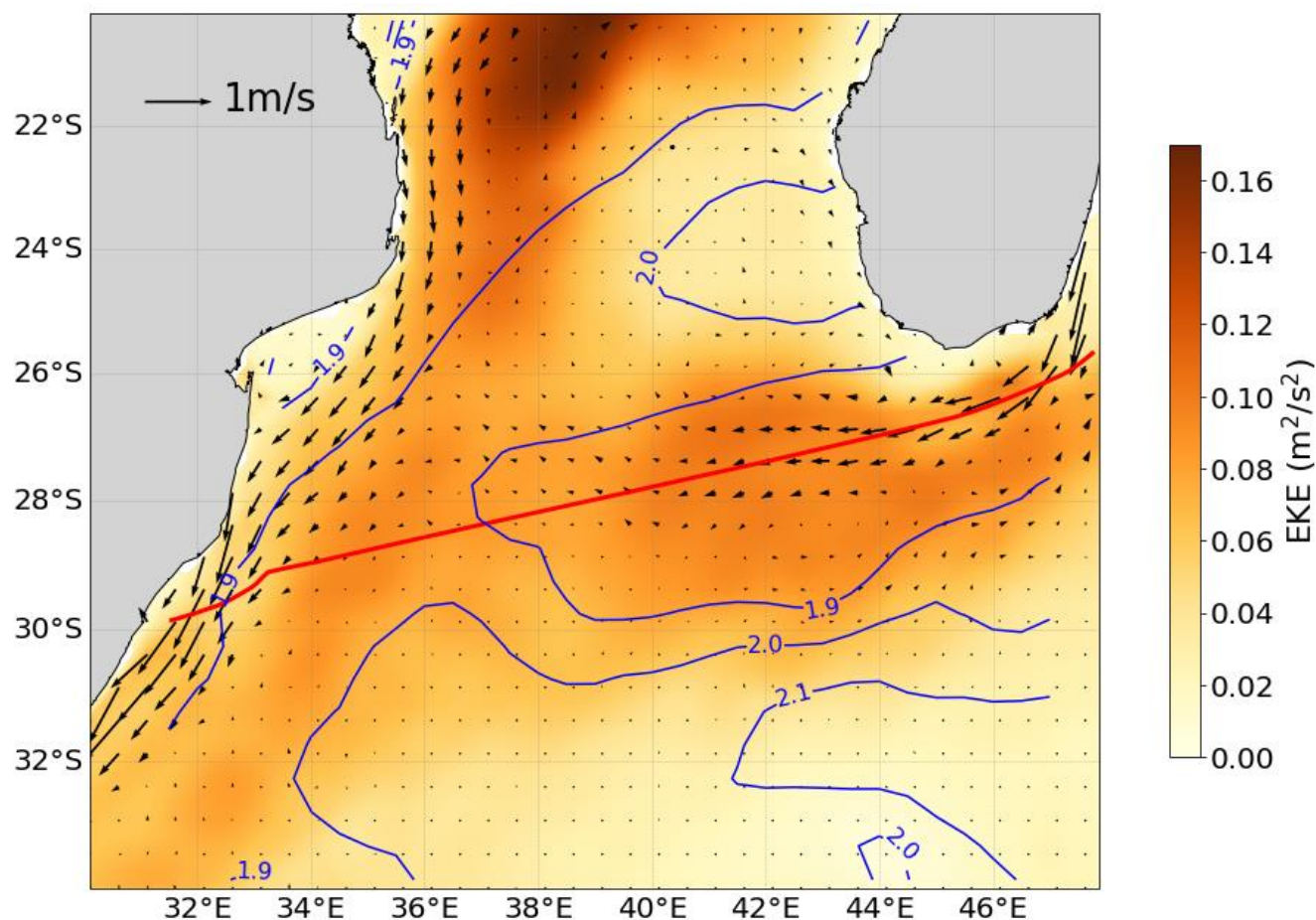


166 leakage (Fig. 2b), implying MHW intensity is closely associated with SST variance (Fig. 2b and e). Weaker SST variance  
167 within the southern MC and along the west coast of Africa, compared to the southernmost open ocean region, also closely  
168 resembles the patterns of MHW duration and cumulative intensity, which suggests that longer (shorter)-lasting and more (less)  
169 severe MHWs are associated with higher (lower) SST variance (Fig. 2b, d, f). Unlike MHW duration, intensity and cumulative  
170 intensity, the mean spatial distribution of MHW frequency reflects an inverse pattern compared to SST variance, suggesting  
171 that where SST variance is high (low), MHWs occur less (more) often (Fig. 2b, c).

172 To investigate the role that underlying oceanographic processes play in driving the observed mean surface MHW  
173 characteristics, mean EKE and geostrophic velocities are shown, with SST variability overlain as contours (Fig. 3). The  
174 westward-flowing SEMC leakage is visible, as is the train of eddies flowing southward through the MC and the fast,  
175 southward-flowing AC (Fig. 1a and 3). EKE is strongest on the western side of the MC and between the southern tip of  
176 Madagascar and the continent, where stronger poleward and south-westerly currents are present (respectively) (Fig. 3).

177 There is a clear relationship between the spatial patterns of the mean surface MHW metrics and EKE (Fig. 2 and 3). Regions  
178 with high EKE ( $0.08 - 0.16 \text{ m}^2/\text{s}^2$ ) align with the regions where, on average, SST variability is relatively low and MHWs occur  
179 more frequently, but are relatively shorter-lived and less intense, suggesting that the presence of energetic eddies increases the  
180 occurrence and then dissipation of MHW events (Fig. 2b and c and Fig. 3). The regular propagation of eddies with mean  
181 surface flow through these regions results in eddies with short residence times consistently passing through the region, causing  
182 frequent MHWs with short lifespans. On the other hand, where EKE is low ( $0.0 - 0.08 \text{ m}^2/\text{s}^2$ ) corresponds to regions where  
183 observed mean SST variability is relatively high and annual mean MHWs occur less frequently but are longer-lasting and more  
184 intense (Fig. 2b and c and Fig. 3).





185

186 **Figure 3:** Mean eddy kinetic energy (EKE), with mean geostrophic velocities overlaid, calculated from high resolution AVISO data for the  
 187 climatological period from 1993–2023. The blue contour lines indicate SST standard deviation (°C) calculated from NOAA optimally  
 188 interpolated sea surface temperature (OISST V2) high resolution (0.25°) gridded SST data for the same period from 1993–2023. The red  
 189 solid line denotes the IX21 XBT transect.

190

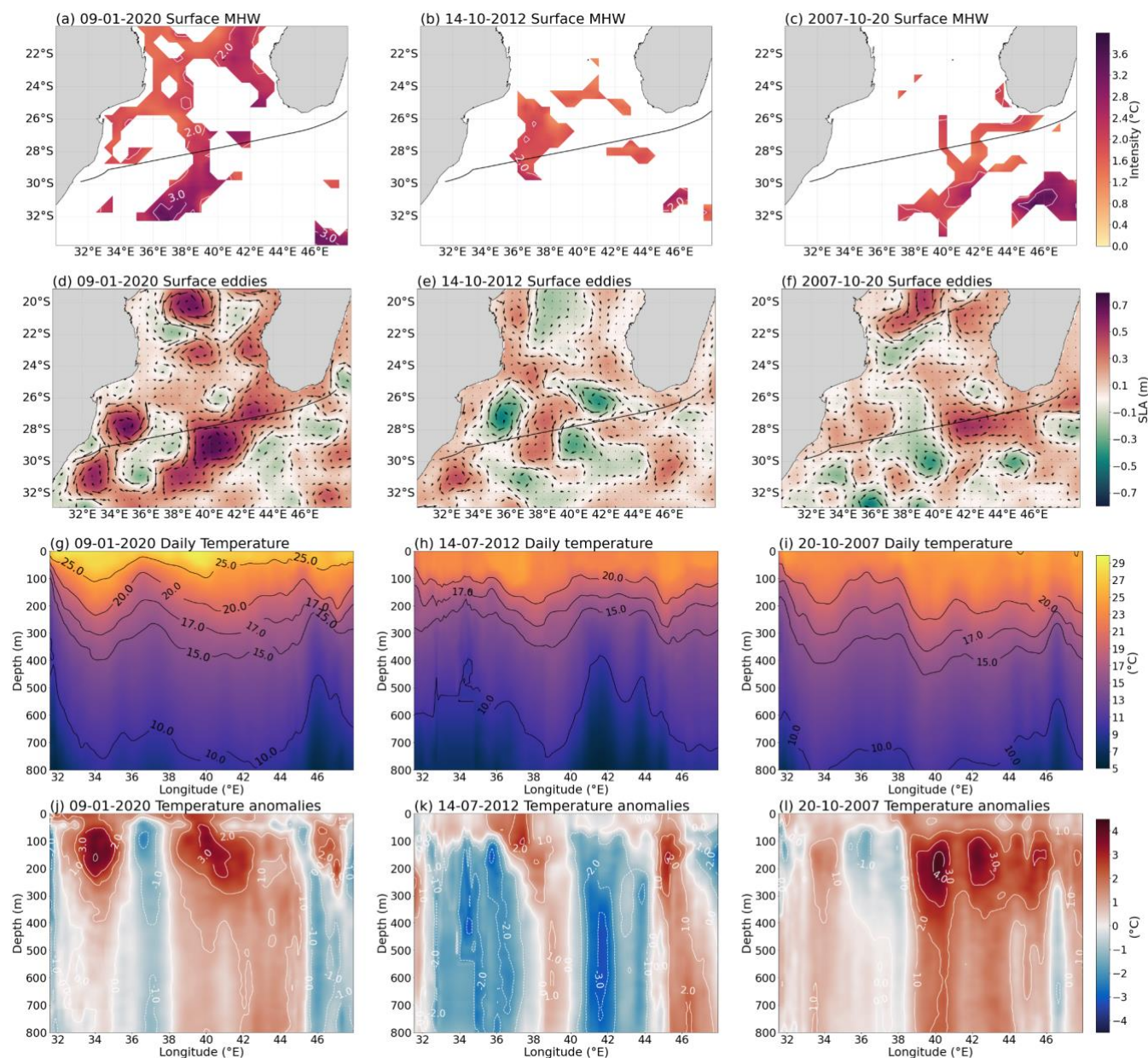
191 The IX21 transect, used in this study to extrapolate *in situ* subsurface data and investigate the subsurface extent of MHWs,  
 192 runs through the SEMC leakage and across the source region of the AC, where eddy activity is high and geostrophic currents  
 193 are strong (Fig. 3). Thus, when investigating the subsurface structure of MHWs along the XBT line, we may capture MHW  
 194 events that are driven by mesoscale eddy activity and occur frequently, but have reduced annual duration, intensity and  
 195 cumulative intensity, compared to the rest of the region.

### 196 3.3 Annual and seasonal surface MHW variability

197 To investigate the subsurface signal of MHWs, we identified when the surface MHWs detected in the SST satellite data were  
 198 co-located with the IX21 XBT line. 65 MHWs of varying intensities and sizes were identified in the SST data on days with



199 corresponding XBT transects. For each day where subsurface data was available and a MHW signal was present over the  
 200 XBT transect, the surface MHW intensity was compared to daily subsurface temperature and anomaly profiles. MHWs that  
 201 occurred on 9 January 2020, 14 July 2012 and 20 October 2007 were selected as case studies (Fig. 4).



202  
 203 **Figure 4:** Surface MHW intensity using OISST V2 data (°C) that took place on (a) 9 January 2020, (b) 14 July 2012, (c) 20 October  
 204 2007. Sea level anomalies (m) and geostrophic current velocities (m/s) on the three MHW case study days (d) 9 January 2020, (e) 20 October  
 205 2007 and (f) 13 July 2012 using optimally interpolated AVISO altimetry satellite data. The black solid line indicates the position of the XBT  
 206 transect (IX21). Subsurface temperature (g - i) and temperature anomalies (j - l) from the 9th - 13th January 2020 (g and j), the 14th - 17th  
 207 July 2012 (h and k) and from the 20<sup>th</sup> - 24th October 2007 (i and l). The subsurface profiles were plotted using in situ XBT data from the  
 208 IX21 transect line (see methods section).



209  
 210 For all three MHW case studies, the spatial distribution of the MHWs are aligned with the spatial distribution of the warm-  
 211 core anticyclonic eddies, with maximum MHW intensities directly surrounding the cores of the largest anticyclonic eddies  
 212 (Fig. 4a - d). For example, for the 9 January 2020 MHW case study, the maximum MHW intensities (3 °C) are identified  
 213 surrounding the largest anticyclonic, with warm core eddies of 0.7 m above sea level, at 27 - 32° S and 36 - 42° E (Fig. 4a  
 214 and d). Likewise, on 14 July 2012 and 20 October 2007, the most intense surface MHW temperatures were recorded (2 °C)  
 215 surrounding the largest sea level anomalies (0.4 - 0.5 m above sea level) (Fig. 4b,c,e and f).  
 216 Moreover, anomalously warm temperatures surrounding warm-core eddies are present with depth at the locations where  
 217 MHWs persist over the XBT transect line (Fig. 4a - c and g - l). During the January 2020 MHW event, two distinct columns  
 218 of anomalously warm temperatures (1 - 4 °C) extend from the surface to 800 m at 34° E and 38 - 45° E (Fig. 4j). At 36 - 38°  
 219 E, the location of the surface-identified July 2012 MHW, anomalously warm water (1 - 2°C) extends from the surface to 800  
 220 m (Fig. 4h). Between 39 - 46° E, the October 2007 MHW has temperature anomalies (1-4°C) that extend below the surface-  
 221 identified MHW to 800 m (Fig. 4l).  
 222 The subsurface temperature anomalies associated with surface-identified MHWs, appear to intensify below the surface (Fig.  
 223 4a,b,c,j,k,l and Table 1). During the January 2020 MHW case study, the subsurface temperature anomalies, relative to the  
 224 surface MHW intensity (2 °C) at 34° E and between 38 - 45° E, are most extreme from 50 - 200 m, reaching up to 4 °C (Fig.  
 225 4a and j and Table 1). Similarly, subsurface temperature anomalies during the October 2007 MHW event reach maximum  
 226 temperatures (4°C) above the seasonal mean below 100 m at 40° E, 42° E and 45° E (Fig. 4l and Table 1). Although much  
 227 weaker, at 38° E, the subsurface temperature anomaly that extends below the surface-identified July 2012 MHW has a  
 228 maximum anomaly of 2 °C that extends from 0 - 150 m (Fig. 4k and Table 1). Given that the mixed layer depth, on average,  
 229 in this region does not exceed 100 m (de Boyer Montégut et al., 2004), the most intense MHW temperatures are experienced  
 230 below the mixed layer, and not at the surface.

231 **Table 1:** Surface and subsurface MHW characteristics for all three case studies: location of surface MHW over XBT transect  
 232 (Location), temperature anomalies (maximum surface intensity (Surface), maximum temperature anomaly (Max) and the depth  
 233 where it occurs (Depth of Max)), SLA at the location of surface-identified MHWs (SLA) where positive indicates the presence  
 234 of a warm core eddy.  
 235

| MHW case studies | Location          | Temperature anomalies |           |                   | SLA (m) |
|------------------|-------------------|-----------------------|-----------|-------------------|---------|
|                  |                   | Surface (°C)          | Max. (°C) | Depth of Max. (m) |         |
| 09-01-2020       | 34° E; 38 - 45° E | 3                     | 4         | 100 - 200         | 0.5     |





---

|            |            |   |   |           |     |
|------------|------------|---|---|-----------|-----|
| 14-07-2012 | 36 – 38° E | 2 | 2 | 100       | 0.2 |
| 20-10-2007 | 39 – 46° E | 2 | 4 | 100 – 200 | 0.4 |

---

236

237 However, weaker subsurface temperature anomalies are associated with warm-core eddies when there is no surface identified  
238 MHW signal (Fig. 4a – l). At 46° E, during both the January 2020 and July 2012 MHW case studies, a weak subsurface  
239 temperature anomaly (1 - 2°C) extends below the surface where no surface MHW was identified, but a warm-core mesoscale  
240 eddy (SLA of 0.2 – 0.4 m) is found (Fig. 4 a,b, j and k). Similarly, between 32 - 36° E during the October 2007 MHW, a weak  
241 column of anomalously warm water (1 – 2 °C) extends from 0 - 800m and is associated with an eddy (SLA of 0.3 m) rather  
242 than a surface identified MHW (Fig. 4c, f and l). Nonetheless, the most extreme subsurface temperature anomalies strongly  
243 reflect the vertical extent of the surface MHW, rather than a warm core eddy signature, as the anomalies associated with surface  
244 identified MHWs and mesoscale eddies are larger than those associated with mesoscale eddies alone (Fig. 4a - c and g - l).  
245 Overall, the three MHW case studies have different spatial distributions and intensities, but there are several commonalities  
246 between all three events (Fig. 4). All three case studies indicate that MHWs are associated with warm-core anticyclonic eddies  
247 and subsurface temperature anomalies that extend down to at least 800m and intensify below the surface typically within the  
248 thermocline.

#### 249 4. Discussion

250 MHWs in the SWIO can be classified as abrupt and intense events, which is typical for highly dynamic WBCs (Marin et al.,  
251 2022). Regions with annual maximum MHW cumulative intensity, which is the integration of MHW duration and intensity,  
252 experience the most severe impacts on marine ecosystems (Holbrook et al., 2020). Southwest of Madagascar, where maximum  
253 cumulative intensity is observed, MHWs have previously caused severe coral bleaching events in one of the largest barrier  
254 reef coral systems, Le Grand Recif Toliara (Mawren et al., 2022 a). Furthermore, the co-occurrence of MHWs and tropical  
255 cyclones across the SWIO causes these extreme events to intensify, which has not only had devastating impacts on southeast  
256 African coastal countries and Madagascar, but has also severely impacted coastal marine ecosystems, especially through the  
257 exacerbation of coral bleaching events off the southeast African coast, where this study showed MHWs are frequent and intense  
258 (Mawren et al., 2022 b). This highlights the importance of studying MHWs in this region as damage to habitat-forming coral  
259 species may have cascading impacts on the entire structure and functioning of the marine ecosystem, which upholds high  
260 marine biodiversity and supports fisheries largely depended upon by the coastal community of Madagascar (Obura, 2012;  
261 Pereira et al., 2014; Obura et al., 2021; Mawren et al., 2022 b).

262 In the SWIO, regions with high eddy activity and lower SST variability experience MHWs that occur frequently, but are  
263 shorter-lived and less intense, whereas regions with low eddy activity, but high SST variability, experience more intense,



264 longer-lasting, but less frequent MHWs. Less intense and shorter-lived MHWs are typical of WBCs with high eddy abundance  
265 (Frölicher et al., 2018; Oliver et al., 2018; Oliver, 2019; Spillman et al., 2021; Fragkopoulou et al., 2023). The passage of  
266 eddies through the MC and from the SEMC largely dictates the growth and decay of MHWs in the SWIO (Bian et al., 2023;  
267 Zhang et al., 2023). On the other hand, more intense, longer-lasting, but less frequent MHWs occur where SST variability is  
268 high, but eddy activity is low and weak surface currents are present. The local processes that drive high SST variability are  
269 known to result in more intense MHWs (Oliver et al., 2018). Since MHWs within WBCs predominantly occur within warm-  
270 core anticyclonic eddies, weak mean flow and high eddy injection southwest of Madagascar and in the region of SEMC  
271 retroflection likely drives higher mean SST variability which establishes, on average, more intense MHWs (Halo et al., 2014).  
272 However, other processes, such as anomalous net surface heat fluxes driven by weaker winds and increased insolation may  
273 also play a role in driving higher SST variability, and thus more intense MHWs, in these regions (Mawren et al., 2022 a).  
274 Furthermore, the presence of mesoscale eddies surrounding surface MHWs during the three selected case studies indicates  
275 that, as is seen in other WBCs, anomalously warm anticyclonic eddies act as a mechanism for MHW intensification (Schaeffer  
276 and Roughan, 2017; Elzahaby et al., 2021; Mawren et al., 2022 a). During the case studies, greatest MHW intensity was present  
277 where anomalously high SLA that exceeded the mean SLA amplitudes (0.3 cm) generally associated with warm-core eddies  
278 in SWIO (Schouten et al., 2003; Swart et al., 2010; Halo et al., 2014). This is significant as WBC systems and their dynamical  
279 processes, such as mesoscale eddies, are intensifying and causing WBC warming to be two to three times faster than the mean  
280 global ocean warming rate (Wu et al., 2012). Intensification of warm-core eddies, under the current WBC warming trends,  
281 may subsequently intensify local SST variability and amplify MHW events in the future (Wu et al., 2012; Schaeffer and  
282 Roughan, 2017; Benthuyesen et al., 2020).

283 The intensification of MHWs in the presence of mesoscale eddies is not limited to the surface, as distinct columns of deep-  
284 reaching and warm temperature anomalies are identified below the surface-identified MHW case studies. Eddies in the SWIO,  
285 can extend to intermediate depths of 800 - 2000m (Quarty and Srokosz, 2004; Halo et al., 2014). We found that subsurface  
286 temperature anomalies associated with MHWs in the SWIO could extend to at least 800m below surface-detected MHWs.  
287 Furthermore, the observed temperature anomalies intensify below the surface, and reach temperatures which exceed the surface  
288 MHW intensities below the MLD, which could also be associated with a deepening of the thermocline (Schaeffer and  
289 Roughan, 2017; Elzahaby and Schaeffer, 2019; Amaya et al., 2023; Fragkopoulou et al., 2023). This suggests that, as is seen  
290 in other WBCs where eddies drive deeper and longer-lasting MHWs, anticyclonic eddies may restrict the horizontal extent of  
291 MHWs in the SWIO and also act to localise the intensity of the MHW within the eddy column, below the surface (Schaeffer  
292 and Roughan, 2017; Elzahaby and Schaeffer, 2019; Elzahaby et al., 2021; Perez et al., 2021; Fragkopoulou et al., 2023; Zhang  
293 et al., 2023). These findings highlight the importance of studying the subsurface extent of MHWs, as exposure of vital coastal  
294 ecosystems to the effects of MHWs may be largely underestimated when only studying MHWs using surface satellite data  
295 (Schaeffer and Roughan, 2017; Elzahaby and Schaeffer, 2019; Benthuyesen et al., 2020; Elzahaby et al., 2021; Zhang et al.,  
296 2023).



297 Overall, we find that mesoscale eddies not only play an important role in dictating the frequency, duration and intensity of  
298 surface MHW events, but the subsurface temperature anomalies also extend below a surface-identified MHW. Thus, the  
299 importance of mesoscale eddies in driving MHW extents in the SWIO is highlighted. However, past heat budget studies of  
300 global MHWs using high-resolution models (Hayashida et al., 2020; Marin et al., 2022) have shown that abrupt and intense  
301 MHWs are likely driven by a mixed combination of processes, such as local advection, eddy heat flux, air-sea heat flux and  
302 large-scale climate modes, which control heat variations over small and different spatio-temporal scales. The high complexity  
303 of the SWIO therefore suggests that, while eddies may act as a catalyst for MHW events, it is likely a combination of different  
304 oceanic and atmospheric processes that drive MHWs, which warrant further investigation.

## 305 **5. Conclusions**

306 To date, our study is the first to describe the subsurface extent of MHWs in the Greater Agulhas Current System, which makes  
307 up the SWIO, and reveals that these events can extend to depths of at least 800 m and exhibit maximum intensity below the  
308 surface. This finding suggests that investigation of MHWs using only surface satellite data may significantly underestimate  
309 the severity and impacts of MHWs. The presence of anticyclonic warm-core eddies appears to influence both the surface  
310 distribution and subsurface signals of MHWs, indicating a complex interaction that warrants further investigation.

311 Our results highlight the need for consistent and long-term subsurface data to better understand the progression, frequency,  
312 and duration of MHWs below the surface. Investigating heat budgets and the drivers of MHWs will provide deeper insights  
313 into the mechanisms behind these events, enhancing the accuracy of forecasting models and improving management strategies  
314 to mitigate the impacts on marine ecosystems.

315 Future research should prioritize specific locations within the SWIO where MHWs are most extreme or frequent, focusing on  
316 areas with high marine biodiversity, such as coral reef systems. These targeted studies will be crucial for understanding local  
317 MHW characteristics and their effects on fisheries and coastal economies, ultimately contributing to more effective  
318 conservation and resource management efforts.

## 319 **Code availability**

320 The code used to detect MHWs is available at <https://github.com/ecjoliver/marineHeatWaves>.

## 321 **Data availability**

322 All data used in this study are open access. The daily NOAA OISST V2 data is available  
323 at <https://coastwatch.pfeg.noaa.gov/erddap/> (Huang et al., 2020). The HR-XBT data is made available by the Scripps





324 Institution of Oceanography HR-XBT program (IX21 - <http://www-hrx.ucsd.edu/ix15.html>) The AVISO product is available  
325 from CMEMS (<https://doi.org/10.48670/moi-00148>, E.U. CMEMS).

### 326 **Author contributions**

327 CBW performed the analysis and led the writing of the manuscript as part of her Honours research project at University of  
328 Cape Town, South Africa. JCS, JS, TM, DM and NM supervised, proposed and guided the project, and contributed to the  
329 writing.

### 330 **Competing interests**

331 The authors declare that they have no conflict of interest.

### 332 **Disclaimer**

### 333 **Acknowledgements**

334 The research leading to these results has received funding from the National Research Foundation (NRF) through Grant  
335 PMDS230630125138, the South African Environmental Observation Network (SAEON) and the University of Cape Town.  
336 JS was supported by the NOAA Global Ocean Monitoring and Observing Program through Award NA20OAR4320278. NM  
337 was supported by Australian Research Council Future Fellowship FT220100475.

### 338 **References**

- 339 Amaya, D. J., Jacox, M. G., Alexander, M. A., Scott, J. D., Deser, C., Capotondi, A., and Phillips, A. S.: Bottom marine  
340 heatwaves along the continental shelves of North America, *Nat. Commun.*, 14, 1038, [https://doi.org/10.1038/s41467-023-](https://doi.org/10.1038/s41467-023-36567-0)  
341 [36567-0](https://doi.org/10.1038/s41467-023-36567-0), 2023.
- 342 Bai, L., Zhu, G., Huang, H., Zhang, L., Lü, H., and Zhang, Y.: Characteristics of mesoscale eddies in the Mozambique Channel,  
343 *PLOS ONE*, 19, e0302367, <https://doi.org/10.1371/journal.pone.0302367>, 2024.
- 344 Banzon, V., Smith, T. M., Chin, T. M., Liu, C., and Hankins, W.: A long-term record of blended satellite and in situ sea-  
345 surface temperature for climate monitoring, modeling and environmental studies, *Earth Syst. Sci. Data*, 8, 165–176,  
346 <https://doi.org/10.5194/essd-8-165-2016>, 2016.
- 347 Beal, L. M., De Ruijter, W. P. M., Biastoch, A., Zahn, R., SCOR/WCRP/IAPSO Working Group 136, Cronin, M., Hermes, J.,  
348 Lutjeharms, J., Quartly, G., Tozuka, T., Baker-Yeboah, S., Bormman, T., Cipollini, P., Dijkstra, H., Hall, I., Park, W., Peeters,



- 349 F., Penven, P., Ridderinkhof, H., and Zinke, J.: On the role of the Agulhas system in ocean circulation and climate, *Nature*,  
350 472, 429–436, <https://doi.org/10.1038/nature09983>, 2011.
- 351 Beal, L. M., Vialard, J., Roxy, M. K., Li, J., Andres, M., Annamalai, H., Feng, M., Han, W., Hood, R., Lee, T., Lengaigne,  
352 M., Lumpkin, R., Masumoto, Y., McPhaden, M. J., Ravichandran, M., Shinoda, T., Sloyan, B. M., Strutton, P. G.,  
353 Subramanian, A. C., Tozuka, T., Ummerhofer, C. C., Unnikrishnan, A. S., Wiggert, J., Yu, L., Cheng, L., Desbruyères, D. G.,  
354 and Parvathi, V.: A Road Map to IndOOS-2: Better Observations of the Rapidly Warming Indian Ocean, *Bull. Am. Meteorol.*  
355 *Soc.*, 101, E1891–E1913, <https://doi.org/10.1175/BAMS-D-19-0209.1>, 2020.
- 356 Benthuisen, J. A., Oliver, E. C. J., Chen, K., and Wernberg, T.: Editorial: Advances in Understanding Marine Heatwaves and  
357 Their Impacts, *Front. Mar. Sci.*, 7, 147, <https://doi.org/10.3389/fmars.2020.00147>, 2020.
- 358 Bian, C., Jing, Z., Wang, H., Wu, L., Chen, Z., Gan, B., and Yang, H.: Oceanic mesoscale eddies as crucial drivers of global  
359 marine heatwaves, *Nat. Commun.*, 14, 2970, <https://doi.org/10.1038/s41467-023-38811-z>, 2023.
- 360 Chandler, M., Zilberman, N. V., and Sprintall, J.: Seasonal to Decadal Western Boundary Current Variability From Sustained  
361 Ocean Observations, *Geophys. Res. Lett.*, 49, e2022GL097834, <https://doi.org/10.1029/2022GL097834>, 2022.
- 362 Chauhan, A., Smith, P. A. H., Rodrigues, F., Christensen, A., St. John, M., and Mariani, P.: Distribution and impacts of long-  
363 lasting marine heat waves on phytoplankton biomass, *Front. Mar. Sci.*, 10, 1177571,  
364 <https://doi.org/10.3389/fmars.2023.1177571>, 2023.
- 365 Collins, C., Reason, C. J. C., and Hermes, J. C.: Scatterometer and reanalysis wind products over the western tropical Indian  
366 Ocean, *J. Geophys. Res. Oceans*, 117, 2011JC007531, <https://doi.org/10.1029/2011JC007531>, 2012.
- 367 DiMarco, S. F., Chapman, P., and Nowlin, W. D.: Satellite observations of upwelling on the continental shelf south of  
368 Madagascar, *Geophys. Res. Lett.*, 27, 3965–3968, <https://doi.org/10.1029/2000GL012012>, 2000.
- 369 Elzahaby, Y. and Schaeffer, A.: Observational Insight Into the Subsurface Anomalies of Marine Heatwaves, *Front. Mar. Sci.*,  
370 6, 745, <https://doi.org/10.3389/fmars.2019.00745>, 2019.
- 371 Elzahaby, Y., Schaeffer, A., Roughan, M., and Delaux, S.: Oceanic Circulation Drives the Deepest and Longest Marine  
372 Heatwaves in the East Australian Current System, *Geophys. Res. Lett.*, 48, e2021GL094785,  
373 <https://doi.org/10.1029/2021GL094785>, 2021.
- 374 Fragkopoulou, E., Sen Gupta, A., Costello, M. J., Wernberg, T., Araújo, M. B., Serrão, E. A., De Clerck, O., and Assis, J.:  
375 Marine biodiversity exposed to prolonged and intense subsurface heatwaves, *Nat. Clim. Change*, 13, 1114–1121,  
376 <https://doi.org/10.1038/s41558-023-01790-6>, 2023.
- 377 Frölicher, T. L., Fischer, E. M., and Gruber, N.: Marine heatwaves under global warming, *Nature*, 560, 360–364,  
378 <https://doi.org/10.1038/s41586-018-0383-9>, 2018.
- 379 Garrabou, J., Gómez-Gras, D., Medrano, A., Cerrano, C., Ponti, M., Schlegel, R., Bensoussan, N., Turicchia, E., Sini, M.,  
380 Gerovasileiou, V., Teixido, N., Mirasole, A., Tamburello, L., Cebrian, E., Rilov, G., Ledoux, J., Souissi, J. B., Khamassi, F.,  
381 Ghanem, R., Benabdi, M., Grimes, S., Ocaña, O., Bazairi, H., Hereu, B., Linares, C., Kersting, D. K., La Rovira, G., Ortega,  
382 J., Casals, D., Pagès-Escolà, M., Margarit, N., Capdevila, P., Verdura, J., Ramos, A., Izquierdo, A., Barbera, C., Rubio-Portillo,



383 E., Anton, I., López-Sendino, P., Díaz, D., Vázquez-Luis, M., Duarte, C., Marbà, N., Aspillaga, E., Espinosa, F., Grech, D.,  
384 Guala, I., Azzurro, E., Farina, S., Cristina Gambi, M., Chimienti, G., Montefalcone, M., Azzola, A., Mantas, T. P., Frascchetti,  
385 S., Ceccherelli, G., Kipson, S., Bakran-Petricioli, T., Petricioli, D., Jimenez, C., Katsanevakis, S., Kizilkaya, I. T., Kizilkaya,  
386 Z., Sartoretto, S., Elodie, R., Ruitton, S., Comeau, S., Gattuso, J., and Harmelin, J.: Marine heatwaves drive recurrent mass  
387 mortalities in the Mediterranean Sea, *Glob. Change Biol.*, 28, 5708–5725, <https://doi.org/10.1111/gcb.16301>, 2022.

388 Goni, G. J., Sprintall, J., Bringas, F., Cheng, L., Cirano, M., Dong, S., Domingues, R., Goes, M., Lopez, H., Morrow, R.,  
389 Rivero, U., Rossby, T., Todd, R. E., Trinanes, J., Zilberman, N., Baringer, M., Boyer, T., Cowley, R., Domingues, C. M.,  
390 Hutchinson, K., Kramp, M., Mata, M. M., Reseghetti, F., Sun, C., Bhaskar Tvs, U., and Volkov, D.: More Than 50 Years of  
391 Successful Continuous Temperature Section Measurements by the Global Expendable Bathythermograph Network, Its  
392 Integrability, Societal Benefits, and Future, *Front. Mar. Sci.*, 6, 452, <https://doi.org/10.3389/fmars.2019.00452>, 2019.

393 Großelindemann, H., Ryan, S., Ummenhofer, C. C., Martin, T., and Biastoch, A.: Marine Heatwaves and Their Depth  
394 Structures on the Northeast U.S. Continental Shelf, *Front. Clim.*, 4, 857937, <https://doi.org/10.3389/fclim.2022.857937>, 2022.

395 Guo, X., Gao, Y., Zhang, S., Wu, L., Chang, P., Cai, W., Zscheischler, J., Leung, L. R., Small, J., Danabasoglu, G., Thompson,  
396 L., and Gao, H.: Threat by marine heatwaves to adaptive large marine ecosystems in an eddy-resolving model, *Nat. Clim.*  
397 *Change*, 12, 179–186, <https://doi.org/10.1038/s41558-021-01266-5>, 2022.

398 Halo, I., Backeberg, B., Penven, P., Ansorge, I., Reason, C., and Ullgren, J. E.: Eddy properties in the Mozambique Channel:  
399 A comparison between observations and two numerical ocean circulation models, *Deep Sea Res. Part II Top. Stud. Oceanogr.*,  
400 100, 38–53, <https://doi.org/10.1016/j.dsr2.2013.10.015>, 2014.

401 Hayashida, H., Matear, R. J., Strutton, P. G., and Zhang, X.: Insights into projected changes in marine heatwaves from a high-  
402 resolution ocean circulation model, *Nat. Commun.*, 11, 4352, <https://doi.org/10.1038/s41467-020-18241-x>, 2020.

403 Hermes, J. C., Masumoto, Y., Beal, L. M., Roxy, M. K., Vialard, J., Andres, M., Annamalai, H., Behera, S., D’Adamo, N.,  
404 Doi, T., Feng, M., Han, W., Hardman-Mountford, N., Hendon, H., Hood, R., Kido, S., Lee, C., Lee, T., Lengaigne, M., Li, J.,  
405 Lumpkin, R., Navaneeth, K. N., Milligan, B., McPhaden, M. J., Ravichandran, M., Shinoda, T., Singh, A., Sloyan, B., Strutton,  
406 P. G., Subramanian, A. C., Thurston, S., Tozuka, T., Ummenhofer, C. C., Unnikrishnan, A. S., Venkatesan, R., Wang, D.,  
407 Wiggert, J., Yu, L., and Yu, W.: A Sustained Ocean Observing System in the Indian Ocean for Climate Related Scientific  
408 Knowledge and Societal Needs, *Front. Mar. Sci.*, 6, 355, <https://doi.org/10.3389/fmars.2019.00355>, 2019.

409 Hobday, A. J. and Pecl, G. T.: Identification of global marine hotspots: sentinels for change and vanguards for adaptation  
410 action, *Rev. Fish Biol. Fish.*, 24, 415–425, <https://doi.org/10.1007/s11160-013-9326-6>, 2014.

411 Hobday, A. J., Alexander, L. V., Perkins, S. E., Smale, D. A., Straub, S. C., Oliver, E. C. J., Benthuyssen, J. A., Burrows, M.  
412 T., Donat, M. G., Feng, M., Holbrook, N. J., Moore, P. J., Scannell, H. A., Sen Gupta, A., and Wernberg, T.: A hierarchical  
413 approach to defining marine heatwaves, *Prog. Oceanogr.*, 141, 227–238, <https://doi.org/10.1016/j.pocean.2015.12.014>, 2016.

414 Holbrook, N. J., Sen Gupta, A., Oliver, E. C. J., Hobday, A. J., Benthuyssen, J. A., Scannell, H. A., Smale, D. A., and Wernberg,  
415 T.: Keeping pace with marine heatwaves, *Nat. Rev. Earth Environ.*, 1, 482–493, <https://doi.org/10.1038/s43017-020-0068-4>,  
416 2020.



- 417 Hu, S., Li, S., Zhang, Y., Guan, C., Du, Y., Feng, M., Ando, K., Wang, F., Schiller, A., and Hu, D.: Observed strong subsurface  
418 marine heatwaves in the tropical western Pacific Ocean, *Environ. Res. Lett.*, 16, 104024, [https://doi.org/10.1088/1748-](https://doi.org/10.1088/1748-9326/ac26f2)  
419 [9326/ac26f2](https://doi.org/10.1088/1748-9326/ac26f2), 2021.
- 420 Marin, M., Feng, M., Bindoff, N. L., and Phillips, H. E.: Local Drivers of Extreme Upper Ocean Marine Heatwaves Assessed  
421 Using a Global Ocean Circulation Model, *Front. Clim.*, 4, 788390, <https://doi.org/10.3389/fclim.2022.788390>, 2022.
- 422 Mawren, D., Hermes, J., and Reason, C. J. C.: Marine heatwaves in the Mozambique Channel, *Clim. Dyn.*, 58, 305–327,  
423 <https://doi.org/10.1007/s00382-021-05909-3>, 2022a.
- 424 Mawren, D., Hermes, J., and Reason, C. J. C.: Marine heat waves and tropical cyclones - Two devastating types of coastal  
425 hazard in South-eastern Africa, *Estuar. Coast. Shelf Sci.*, 277, 108056, <https://doi.org/10.1016/j.ecss.2022.108056>, 2022a.
- 426 Mills, K., Pershing, A., Brown, C., Chen, Y., Chiang, F.-S., Holland, D., Lehuta, S., Nye, J., Sun, J., Thomas, A., and Wahle,  
427 R.: Fisheries Management in a Changing Climate: Lessons From the 2012 Ocean Heat Wave in the Northwest Atlantic,  
428 *Oceanography*, 26, <https://doi.org/10.5670/oceanog.2013.27>, 2013.
- 429 Obura, D.: The Diversity and Biogeography of Western Indian Ocean Reef-Building Corals, *PLoS ONE*, 7, e45013,  
430 <https://doi.org/10.1371/journal.pone.0045013>, 2012.
- 431 Obura, D., Gudka, M., Samoilys, M., Osuka, K., Mbugua, J., Keith, D. A., Porter, S., Roche, R., Van Hooidek, R., Ahamada,  
432 S., Araman, A., Karisa, J., Komakoma, J., Madi, M., Ravinia, I., Razafindrainibe, H., Yahya, S., and Zivane, F.: Vulnerability  
433 to collapse of coral reef ecosystems in the Western Indian Ocean, *Nat. Sustain.*, 5, 104–113, [https://doi.org/10.1038/s41893-](https://doi.org/10.1038/s41893-021-00817-0)  
434 [021-00817-0](https://doi.org/10.1038/s41893-021-00817-0), 2021.
- 435 Oliver, E. C. J.: Mean warming not variability drives marine heatwave trends, *Clim. Dyn.*, 53, 1653–1659,  
436 <https://doi.org/10.1007/s00382-019-04707-2>, 2019.
- 437 Oliver, E. C. J., Donat, M. G., Burrows, M. T., Moore, P. J., Smale, D. A., Alexander, L. V., Benthuisen, J. A., Feng, M., Sen  
438 Gupta, A., Hobday, A. J., Holbrook, N. J., Perkins-Kirkpatrick, S. E., Scannell, H. A., Straub, S. C., and Wernberg, T.: Longer  
439 and more frequent marine heatwaves over the past century, *Nat. Commun.*, 9, 1324, [https://doi.org/10.1038/s41467-018-](https://doi.org/10.1038/s41467-018-03732-9)  
440 [03732-9](https://doi.org/10.1038/s41467-018-03732-9), 2018.
- 441 Oliver, E. C. J., Benthuisen, J. A., Darmaraki, S., Donat, M. G., Hobday, A. J., Holbrook, N. J., Schlegel, R. W., and Sen  
442 Gupta, A.: Marine Heatwaves, *Annu. Rev. Mar. Sci.*, 13, 313–342, <https://doi.org/10.1146/annurev-marine-032720-095144>,  
443 2021.
- 444 Pereira, M., Litulo, C., Santos, R., Leal, M., Fernandes, R., Tibiriçá, Y., Williams, J., Atanassov, B., Carreira, F., Massingue,  
445 A., and Silva, I. M. D.: Mozambique marine ecosystems review, <https://doi.org/10.13140/2.1.2092.5766>, 2014.
- 446 Perez, E., Ryan, S., Andres, M., Gawarkiewicz, G., Ummenhofer, C. C., Bane, J., and Haines, S.: Understanding physical  
447 drivers of the 2015/16 marine heatwaves in the Northwest Atlantic, *Sci. Rep.*, 11, 17623, [https://doi.org/10.1038/s41598-021-](https://doi.org/10.1038/s41598-021-97012-0)  
448 [97012-0](https://doi.org/10.1038/s41598-021-97012-0), 2021.
- 449 Phillips, H. E., Tandon, A., Furue, R., Hood, R., Ummenhofer, C. C., Benthuisen, J. A., Menezes, V., Hu, S., Webber, B.,  
450 Sanchez-Franks, A., Cherian, D., Shroyer, E., Feng, M., Wijesekera, H., Chatterjee, A., Yu, L., Hermes, J., Murtugudde, R.,



- 451 Tozuka, T., Su, D., Singh, A., Centurioni, L., Prakash, S., and Wiggert, J.: Progress in understanding of Indian Ocean  
452 circulation, variability, air–sea exchange, and impacts on biogeochemistry, *Ocean Sci.*, 17, 1677–1751,  
453 <https://doi.org/10.5194/os-17-1677-2021>, 2021.
- 454 Quartly, G. D. and Srokosz, M. A.: Eddies in the southern Mozambique Channel, *Deep Sea Res. Part II Top. Stud. Oceanogr.*,  
455 51, 69–83, <https://doi.org/10.1016/j.dsr2.2003.03.001>, 2004.
- 456 Reynolds, R. W., Smith, T. M., Liu, C., Chelton, D. B., Casey, K. S., and Schlax, M. G.: Daily High-Resolution-Blended  
457 Analyses for Sea Surface Temperature, *J. Clim.*, 20, 5473–5496, <https://doi.org/10.1175/2007JCLI1824.1>, 2007.
- 458 Roxy, M. K., Ritika, K., Terray, P., and Masson, S.: The Curious Case of Indian Ocean Warming, *J. Clim.*, 27, 8501–8509,  
459 <https://doi.org/10.1175/JCLI-D-14-00471.1>, 2014.
- 460 Saranya, J. S., Roxy, M. K., Dasgupta, P., and Anand, A.: Genesis and Trends in Marine Heatwaves Over the Tropical Indian  
461 Ocean and Their Interaction With the Indian Summer Monsoon, *J. Geophys. Res. Oceans*, 127, e2021JC017427,  
462 <https://doi.org/10.1029/2021JC017427>, 2022.
- 463 Scannell, H. A., Johnson, G. C., Thompson, L., Lyman, J. M., and Riser, S. C.: Subsurface Evolution and Persistence of Marine  
464 Heatwaves in the Northeast Pacific, *Geophys. Res. Lett.*, 47, e2020GL090548, <https://doi.org/10.1029/2020GL090548>, 2020.
- 465 Schaeffer, A. and Roughan, M.: Subsurface intensification of marine heatwaves off southeastern Australia: The role of  
466 stratification and local winds, *Geophys. Res. Lett.*, 44, 5025–5033, <https://doi.org/10.1002/2017GL073714>, 2017.
- 467 Schaeffer, A., Sen Gupta, A., and Roughan, M.: Seasonal stratification and complex local dynamics control the sub-surface  
468 structure of marine heatwaves in Eastern Australian coastal waters, *Commun. Earth Environ.*, 4, 304,  
469 <https://doi.org/10.1038/s43247-023-00966-4>, 2023.
- 470 Schouten, M. W., De Ruijter, W. P. M., Van Leeuwen, P. J., and Ridderinkhof, H.: Eddies and variability in the Mozambique  
471 Channel, *Deep Sea Res. Part II Top. Stud. Oceanogr.*, 50, 1987–2003, [https://doi.org/10.1016/S0967-0645\(03\)00042-0](https://doi.org/10.1016/S0967-0645(03)00042-0), 2003.
- 472 Sen Gupta, A., Thomsen, M., Benthuisen, J. A., Hobday, A. J., Oliver, E., Alexander, L. V., Burrows, M. T., Donat, M. G.,  
473 Feng, M., Holbrook, N. J., Perkins-Kirkpatrick, S., Moore, P. J., Rodrigues, R. R., Scannell, H. A., Taschetto, A. S.,  
474 Ummenhofer, C. C., Wernberg, T., and Smale, D. A.: Drivers and impacts of the most extreme marine heatwave events, *Sci.*  
475 *Rep.*, 10, 19359, <https://doi.org/10.1038/s41598-020-75445-3>, 2020.
- 476 Spillman, C. M., Smith, G. A., Hobday, A. J., and Hartog, J. R.: Onset and Decline Rates of Marine Heatwaves: Global Trends,  
477 Seasonal Forecasts and Marine Management, *Front. Clim.*, 3, 801217, <https://doi.org/10.3389/fclim.2021.801217>, 2021.
- 478 Swart, N. C., Lutjeharms, J. R. E., Ridderinkhof, H., and De Ruijter, W. P. M.: Observed characteristics of Mozambique  
479 Channel eddies, *J. Geophys. Res. Oceans*, 115, 2009JC005875, <https://doi.org/10.1029/2009JC005875>, 2010.
- 480 Voldsund, A., Aguiar-González, B., Gammelsrød, T., Krakstad, J.-O., and Ullgren, J.: Observations of the East Madagascar  
481 Current system: Dynamics and volume transports, *J. Mar. Res.*, 75, 531–555, <https://doi.org/10.1357/002224017821836725>,  
482 2017.



483 Wu, L., Cai, W., Zhang, L., Nakamura, H., Timmermann, A., Joyce, T., McPhaden, M. J., Alexander, M., Qiu, B., Visbeck,  
484 M., Chang, P., and Giese, B.: Enhanced warming over the global subtropical western boundary currents, *Nat. Clim. Change*,  
485 2, 161–166, <https://doi.org/10.1038/nclimate1353>, 2012.

486 Wyatt, A. S. J., Leichter, J. J., Washburn, L., Kui, L., Edmunds, P. J., and Burgess, S. C.: Hidden heatwaves and severe coral  
487 bleaching linked to mesoscale eddies and thermocline dynamics, *Nat. Commun.*, 14, 25, [https://doi.org/10.1038/s41467-022-](https://doi.org/10.1038/s41467-022-35550-5)  
488 35550-5, 2023.

489 Zhang, Y., Du, Y., Feng, M., and Hobday, A. J.: Vertical structures of marine heatwaves, *Nat. Commun.*, 14, 6483,  
490 <https://doi.org/10.1038/s41467-023-42219-0>, 2023.

491 Zhao, Z., Holbrook, N. J., and Oliver, E. C. J.: An eddy pathway to marine heatwave predictability off eastern Tasmania, *Front.*  
492 *Clim.*, 4, 907828, <https://doi.org/10.3389/fclim.2022.907828>, 2022.

493